

3D MAPPING OF CDM SUBSTRUCTURE AT SUBMILLIMETER WAVELENGTHS

KAIKI TARO INOUE¹ AND MASASHI CHIBA²
kinoue@kindai.phys.ac.jp, chiba@astr.tohoku.ac.jp
Draft version February 7, 2020

ABSTRACT

The Cold Dark Matter (CDM) structure formation model predicts that about 5-10 percent of a typical galactic halo mass $\sim 10^{12}M_{\odot}$ is in substructures with a mass $\lesssim 10^8M_{\odot}$. To directly detect such substructures, we propose to observe dust continuum emission from a strongly lensed QSO-host galaxy using a large submillimeter interferometer array with a high angular resolution ~ 0.01 arcsec such as the planned Atacama Large Submillimeter Array (ALMA). To assess their observational feasibility, we numerically simulate millilensing of an extended circular source by a CDM substructure modeled as a tidally truncated singular isothermal sphere (SIS) embedded in a typical QSO-galaxy lens system B1422+231 modeled as a singular isothermal ellipsoid (SIE) with an external constant shear and a constant convergence. Assuming an angular resolution 0.01 arcsec, we find that angular position of $\sim 10^8M_{\odot}$ substructures at several kpc from the center of the macrolens halo can be directly measured if the size of dust continuum emission region and the gradient of surface brightness at the position of the perturber are sufficiently large. From astrometric shift on scale of a few 10 mas of an image perturbed by a subhalo with respect to an unperturbed macrolensed image, we can break degeneracy between a subhalo mass and a distance provided that macrolensing parameters are determined from positions and fluxes of multiple images.

Subject headings: cosmology: theory – dark matter – gravitational lensing – large-scale structure of universe

1. INTRODUCTION

Recent high-resolution N-body simulations of the CDM structure formation model show an excess in the number of subhalos (“substructures”) in a galaxy-sized halo in comparison with the number of Milky Way or M31 satellites (Klypin et al. 1999; Moore et al. 1999). If the CDM-based structure formation scenario is the correct one, then we expect a large number of invisible satellites inside a halo of galaxies.

Currently, gravitational lensing is the only probe that can test the abundance of these invisible satellites or equivalently, substructures in a galaxy-sized halo. In fact, gravitationally multiply lensed QSOs have recently been used for putting a limit on the surface density and the mass of such invisible substructures (Mao & Schneider 1998; Metcalf & Madau 2001; Chiba 2002; Metcalf & Zhao 2002; Dalal & Kochanek 2002; Bradac et al. 2002). Statistical analyses on these quadruple QSO-galaxy lensing systems that show an anomalous flux ratio imply presence of substructures along the line-of-sight (l.o.s) to the multiple images (Metcalf & Zhao 2001; Evans & Witt 2002; Keeton, Gaudi, & Petters 2003).

However, the location of a subhalo along the l.o.s is poorly constrained. In fact, more massive extragalactic $10^{8-9}M_{\odot}$ halos along the l.o.s to the multiple images may also significantly contribute to altering the flux ratio of multiple images (Metcalf 2004). In order to determine the distances to these subhalos, we need to have more information in addition to the position and flux of multiple images (Yonehara, Susa, & Umemura 2003).

To directly map out the 3D locations of 10^8M_{\odot} invisible subhalos, we propose to observe dust continuum emission from a strongly lensed QSO-host galaxy using a large submillimeter interferometer array with a high angular resolution ~ 0.01 arcsec such as the ALMA.

Recent submillimeter observation revealed that about 60 percent of strongly lensed AGNs are luminous at a submillimeter

wavelength $850\mu\text{m}$ (Barvainis & Ivison 2002) implying that a large amount of energy emitted by stars and AGNs in QSO-host galaxy has been absorbed by dust grains and then re-radiated at longer wavelengths. The dust is heated to temperatures of 20-50K and radiates as a modified blackbody at far-infrared wavelengths (Wiklind 2003). At redshift $z = 3 \sim 4$, the corresponding energy peak is at submillimeter $\sim 0.1\text{mm}$. The dust has a typical scale of 10^2pc to a few kpc. Therefore, the effects of an extended source with angular size larger than the Einstein radius of a perturber will be easily observed at submillimeter wavelengths (Blain 1999; Wiklind & Alloin 2002).

In this *Letter*, we show our simulation results of millilensing of an extended circular source by a CDM substructure whose Einstein radius is smaller than the source size. We also show that astrometric shifts of images perturbed by a subhalo can reveal the 3D position of a subhalo along the l.o.s. As an example, we choose a typical QSO-galaxy lensing system B1422+231 with cusp-caustics in order to check observational feasibility of mapping substructures.

2. SIMULATION

A typical QSO-galaxy lensing system B1422+231 shows an anomalous flux ratio. The images consist of three highly magnified images A, B, and C, and a faint one D located near the lens galaxy. Observed mid-infrared flux ratios are $A/|B| = 0.94 \pm 0.05$, $C/|B| = 0.57 \pm 0.06$, respectively (Chiba, et al. 2005, preprint). The radio and the optical flux ratios are consistent with the mid-infrared values within a ~ 10 percent error. If we assume that the gravitational potential of the macrolens is a smooth one, we expect a cusp-caustic relation in the flux ratio $f \equiv (A+B+C)/(|A|+|B|+|C|) = 0$. However, B1422+231 shows a 20 percent deviation from the $f = 0$ relation. Assuming that such an anomaly is caused by a presence of an SIS perturber in the macrolens halo, the anomaly might be in image A (Dobler & Keeton 2005). The redshifts of the source and

¹ Department of Science and Engineering, Kinki University, Higashi-Osaka, 577-8502, Japan

² Astronomical Institute, Tohoku University, Sendai 980-8578, Japan

the lens are $z_S = 3.62$ and $z_L = 0.34$, respectively. In what follows, we assume the following cosmological parameters: the present density of matter, $\Omega_m = 0.3$, the present density of cosmological constant $\Omega_\Lambda = 0.7$, the Hubble parameter, $h = 0.7$, which yields the angular diameter distance to the lens and to the source, $D_L = 1.00$ Gpc and $D_S = 1.49$ Gpc, respectively.

To model the macrolens system, we adopt an SIE in an external shear field in which the isopotential curves in the projected surface perpendicular to the l.o.s are ellipse (Kormann et al. 1994). For further detail, see Chiba (2002). In what follows, we assume an angular resolution of 0.01 arcsec that will be achieved by the planned *ALMA* at $850 \mu\text{m}$. Because an Einstein radius for an SIS with one-dimensional velocity dispersion σ at $D_L = 1.00$ Gpc and $D_S = 1.49$ Gpc is

$$\theta_{Ep} = 1.0 \times 10 \left(\frac{\sigma}{21 \text{ km/sec}} \right)^2 \text{ mas}, \quad (1)$$

observation with angular resolution of 0.01 arcsec will reveal subhalos with one-dimensional velocity dispersion $\sigma \gtrsim 20$ km/s for B1422+231.

As a model of CDM subhalo, we consider a spherically symmetric tidally truncated SIS with one dimensional velocity dispersion σ . At distance r from the center of a macrolens galactic halo with one dimensional velocity dispersion σ_0 , the tidal radius is approximately given by $r_t \approx r\sigma/\sigma_0$. In the following, we also assume that a perturbing subhalo is located at a distance equal to the size of the Einstein ring of the macrolens halo $D_L\theta_E = 3.8$ kpc from the macrolens center. For an SIS with one dimensional velocity dispersion $\sigma \sim 20$ km/s, the tidally truncated mass is $M_{\text{SIS}} \sim 10^8 M_\odot$.

In our simulation, we put a tidally truncated SIS with a mass $2 \times 10^8 M_\odot$ near the A image³. The corresponding Einstein radius of an SIS is $\theta_{Ep} \sim 17$ mas. As a model of emission from cold dusts, we assume a circularly symmetric Gaussian source with a standard deviation $L = 2.5 \times 10^2$ pc.

3. RESULT

The left panels in figure 1 show lensed images without any perturbers whereas the right panels show those perturbed by an SIS perturber. As shown in a zoomed up picture of an image A (upper right), the angular position of an SIS can be clearly identified by a dipole structure that consists of a pair of dark and bright spot at the place where the surface brightness gradient is non-vanishing (Inoue & Chiba 2003). One can also notice that shifts of an image outside the Einstein radius θ_{Ep} of an SIS with respect to the unperturbed macrolensed image are suppressed (upper left).

If we approximate the lens system near the perturber locally as an SIS plus a constant shear γ and a constant convergence κ , then the lens equation normalized by the Einstein radius θ_{Ep} of an SIS in the coordinates aligned to the shear can be written in terms of a source position $\mathbf{y} = (y_1, y_2)$ and an image position $\mathbf{x} = (x_1, x_2)$, the lens equation (2) as

$$\mathbf{y} = (\mathbf{1} - \Gamma)\mathbf{x} - \frac{\mathbf{x}}{|\mathbf{x}|}, \quad (2)$$

where

$$\Gamma = \begin{pmatrix} \kappa + \gamma & 0 \\ 0 & \kappa - \gamma \end{pmatrix}. \quad (3)$$

Let $\mathbf{x}_0 = (x_{01}, x_{02})$ be the image position for a macrolens model without any perturbers. In terms of the polar coordinates (R_p, ϕ)

defined as $\mathbf{x} = (R_p \cos \phi, R_p \sin \phi)$, the lens equation (2) yields

$$x_{01}^2 (R_p - \xi_2^{-1})^2 + x_{02}^2 (R_p - \xi_1^{-1})^2 = (R_p - \xi_1^{-1})^2 (R_p - \xi_2^{-1})^2, \quad (4)$$

where $\xi_1 \equiv 1 - \kappa - \gamma$ and $\xi_2 \equiv 1 - \kappa + \gamma$. The astrometric shift $\Delta \mathbf{x} \equiv \mathbf{x} - \mathbf{x}_0$ as a function of \mathbf{x}_0 can be obtained by solving a fourth-order equation (4) with equation (2) analytically. For a positive parity case $\xi_1 > 0, \xi_2 > 0$, an image at a horizontal axis $(x_{01}, 0)$ is shifted to $(x_{01} + \xi_1^{-1}, 0)$ whereas an image at a vertical axis $(0, x_{02})$ is shifted to $(0, x_{02} + \xi_2^{-1})$ (Inoue & Chiba 2004). One can see in the upper-right panel in figure 1 that an image A with positive parity $\kappa \sim 0.38, \gamma \sim 0.47$ is largely stretched in the tangential direction by $\xi_1^{-1} \sim 6.7$ and slightly stretched in the radial direction by $\xi_2^{-1} \sim 0.92$ with respect to the center of the perturber. The astrometric shift is significantly suppressed if the lensed image is placed outside the tidal radius centered at an SIS perturber because the projected gravitational potential decreases faster as R^{-1} than an SIS without truncation, where R is the projected distance from the center of the SIS. If the redshift and the one-dimensional velocity dispersion σ_0 of the macrolens halo is known, then we obtain the tidal radius as a function of a distance from the center of the macrolens halo. From the observed angular size for which the astrometric shifts are significantly suppressed, we can determine the distance from the center of the lens halo, in principle.

Next, we show that a measurement of astrometric shift can break degeneracy between a substructure mass and a distance in the l.o.s to the image. Suppose a halo at redshift $z = z_h$ and a clump (a substructure) in the foreground of a halo at redshift $z_c < z_h$. Let D_s, D_{ch}, D_{cs} , and D_h be an angular diameter distance to a source, between a clump and a halo, between a clump and a source, and to a halo, respectively. Provided that the angle between a perturber and the macrolensed image is sufficiently small in comparison with the Einstein radius of the macrolens θ_E , the effective lens equation for an SIS plus a constant shear and a constant convergence can be written as (Keeton 2003)

$$\tilde{\mathbf{y}} = (\mathbf{1} - \tilde{\Gamma})\mathbf{x} - \frac{\mathbf{x}}{|\mathbf{x}|}, \quad (5)$$

where $\tilde{\mathbf{y}} = (\mathbf{1} - \beta\Gamma)^{-1}\mathbf{y}$, $\tilde{\Gamma} = \mathbf{1} - (\mathbf{1} - \beta\Gamma)^{-1}(\mathbf{1} - \Gamma)$ and $\beta = D_{ch}D_s/D_{cs}D_h$. Because an effective unperturbed image position $\tilde{\mathbf{x}}_0$ that satisfies $\tilde{\mathbf{y}} = (\mathbf{1} - \tilde{\Gamma})\tilde{\mathbf{x}}_0$ is equal to the unperturbed macrolensed image position \mathbf{x}_0 , astrometric shifts can be written as $\Delta \mathbf{x} = \mathbf{x} - \tilde{\mathbf{x}}_0$. The effective convergence and shear in $\tilde{\Gamma}$ are then (Keeton 2003)

$$\kappa_{\text{eff}} = \frac{(1-\beta)(\kappa - \beta(\kappa^2 - \gamma^2))}{(1-\beta\kappa)^2 - \beta^2\gamma^2}, \gamma_{\text{eff}} = \frac{(1-\beta)\gamma}{(1-\beta\kappa)^2 - \beta^2\gamma^2}. \quad (6)$$

Thus, astrometric shifts are described in a same manner as in the case $\beta = 0$. A tangential shift is $\Delta x_1 = (1 - \kappa_{\text{eff}} - \gamma_{\text{eff}})^{-1}$ and a radial shift is $\Delta x_2 = (1 - \kappa_{\text{eff}} + \gamma_{\text{eff}})^{-1}$ (Inoue & Chiba 2004). As shown in figure 2, for images with positive parity, the tangential shift decreases as the distance between a perturber and a macrolens halo increases. As the distance to the clump D_c decreases, the astrometric shift becomes less conspicuous and more isotropic. In fact, in the limit $D_c \rightarrow 0$ or equivalently, $\beta \rightarrow 1$, the astrometric shifts converge to a perfect isotropic shift $\Delta \mathbf{x} = \mathbf{x}_0/|\mathbf{x}_0|$. Thus, the distance between a halo and a clump can be measured by the absolute value and the anisotropy of the shifts provided that the distance to the macrolens halo D_h and the source D_s has been known already.

³ We choose an appropriate position of an SIS which approximately gives the observed anomaly flux ratio but we did not fix the relative position of the images in a small source-size limit. Our simulation should be interpreted as a demonstration of extended source-size effects rather than that of a best-fit model.

Similarly, we can calculate astrometric shifts $\Delta \mathbf{x}$ in the background case $z_c > z_h$. Again, the effective lens equation takes the same form as in equation (5) (Keeton 2003),

$$\mathbf{y} = (\mathbf{1} - \tilde{\Gamma})\tilde{\mathbf{x}} - \frac{\tilde{\mathbf{x}}}{|\tilde{\mathbf{x}}|}, \quad (7)$$

where $\tilde{\mathbf{x}} = (\mathbf{1} - \beta\Gamma)\mathbf{x}$, $\tilde{\Gamma} = \mathbf{1} - (\mathbf{1} - \Gamma)(\mathbf{1} - \beta\Gamma)^{-1}$ and $\beta = D_{ch}D_s/D_cD_{sh}$ (D_{sh} is an angular diameter distance between a source and a halo). We can define an effective position of unperturbed image $\tilde{\mathbf{x}}_0$ satisfying $\mathbf{y} = (\mathbf{1} - \tilde{\Gamma})\tilde{\mathbf{x}}_0$, that leads to $\tilde{\mathbf{x}}_0 = (\mathbf{1} - \beta\Gamma)\mathbf{x}_0$. Then astrometric shifts can be expressed as $\Delta \mathbf{x} = (\mathbf{1} - \beta\Gamma)^{-1}\Delta \tilde{\mathbf{x}}((\mathbf{1} - \beta\Gamma)\mathbf{x}_0)$, where $\Delta \tilde{\mathbf{x}} \equiv \tilde{\mathbf{x}} - \tilde{\mathbf{x}}_0$. Thus, astrometric shifts in the background case are different for those in the foreground case with the same β though the effective lens equation takes the same form in both the cases. From the right panels in Figure 2 and 3, one can see that the shifts of images near the horizontal axis ($x_1, 0$) are larger for the background case in comparison with the foreground case with the same β . As shown in the left panel in Figure 2 and panels in Figure 3, the astrometric shift of images on the horizontal axis $\Delta \mathbf{x} = (\xi_1^{-1}, 0)$ and those on the vertical axis $\Delta \mathbf{x} = (0, \xi_2^{-1})$ do not depend on β in the background case. However, astrometric shifts of all the other images do depend on β . As β increases from 0, astrometric shifts tend to become isotropic except for images on the axes of coordinates aligned to the shear but they cannot be perfectly isotropic as in the foreground case even if $\beta = 1$.

4. OBSERVATIONAL FEASIBILITY

The observed values of flux density at $850\mu\text{m}$ of QSOs at $z = 3-4$ with starburst are typically several tens of mJy that implies an emission from dust with temperature 30-60K from a fairly extended region with 10^{2-3} pc (Barvainis & Ivison 2002). Let us assume that the far infrared dust emission can be represented by a single temperature greybody emission with a rest-frame SED (Wiklind 2003)

$$S(\nu_r, T_d) = \Omega B(\nu_r, T_d)(1 - \exp(-\nu_r/\nu_0)^\beta), \quad (8)$$

where $B(\nu_r, T_d)$ is the Planck function in terms of a rest-frame frequency ν_r and a dust temperature T_d , and $\beta = 1-2$ is the model parameter that controls the grain emissivity, ν_0 is the critical frequency that controls the opacity of the dust, and Ω is the solid angle of the source seen from an observer. A rest-frame SED S is related to an observer-frame SED as $\tilde{S}(\nu) = S((1+z)\nu, T_d)/(1+z)$ Assuming a model with $\beta = 1.5$, $\nu_0 = 6\text{THz}$, a dust temperature $T_d = 40\text{K}$ and a dust emission region from a circular disk with a radius $L = 250$ pc, at $850\mu\text{m}$ the observed energy density would be ~ 2.6 mJy.

Because the ratio of the area D within the Einstein radius of a $2 \times 10^8 M_\odot$ SIS perturber to the area of image A is approximately $\sim 1/50$, the observed energy flux from the area D will be $\sim 4 \times 10^{-4}$ Jy taking a magnification factor ~ 6 into account. In order to measure the difference in the energy flux at the scale of the Einstein radius of the SIS perturber, for a source with smooth surface brightness distribution, (e.g. gaussian) one needs a sensitivity at least $\sim 4 \times 10^{-5}$ Jy. On the other hand, the sensitivity of ALMA at $850\mu\text{m}$ for a point source ($S/N=1$) is $1.2 \times 10^{-5} \times (\text{integration time}/5\text{hour})^{-1/2}$ Jy⁴. Thus the ALMA has a sufficient sensitivity for a source with spatially varying surface brightness to detect the dipole structure caused by a $2 \times 10^8 M_\odot$ SIS perturber. The required integration time would be several hours.

5. SUMMARY AND DISCUSSION

In this Letter, we have proposed a new method to realize 3D mapping of CDM substructures in extragalactic halos. We have shown that at submillimeter wavelengths, a measurement of astrometric shifts of perturbed multiple images with respect to unperturbed images can break degeneracy between a subhalo mass and a position in the l.o.s to the image if resolved at scale of an Einstein radius of the perturber. Furthermore, assuming that the tidal radius is approximately equal to the subhalo size, the distance from the center of the macrolens halo can be determined from the size of region within an image outside which the astrometric shift is suppressed.

Although we have considered a very simple model, the essential features of astrometric shifts will not be dramatically altered even if we consider a more complicated model with a number of non-circular subhalos with an NFW profile (Navarro, Frenk & White 1996). This is because (1) The astrometric shifts caused by a significant number of smaller mass subhalos are cancelled out on larger scales if they are not clustered on that scale. However, a several number of massive perturbers (often not within the image) may affect the distortion of images so that the accuracy in measuring the distance to a single perturber along the l.o.s may become significantly worsen. (2) Deviation from a circular symmetry or an SIS mass profile can affect the astrometric shifts significantly. However, the generic feature of dependence on the parity of macrolensed image will probably not be dramatically altered. By increasing the sample number of the internal position within the source, we can make a distinction between the simple model and more sophisticated (complicated) model.

REFERENCES

- Barvainis, R. & Ivison, R., 2002, ApJ, 571, 712
 Bradac, M., Schneider, P., Steinmetz, M., Lombardi, M., & King, L. J., 2002, A&A, 388, 373
 Blain, A. W., MNRAS, 2002, Astrophys. Space Sci., 266, 261
 Chiba, M. 2002, ApJ, 565, 17
 Chiba, M., Minezaki, T., Kashikawa, N., Kataza, H., & Inoue, K. T., 2005, (preprint)
 Dalal, N. & Kochanek, C. S. 2002, ApJ, 572, 25
 Dobler, G. & Keeton, R. C. 2005, astro-ph/0502436
 Evans, N. W. & Witt, H. J. 2003, MNRAS, 345 1351
 Inoue, K. T. & Chiba, M. 2003, ApJL, 591, L83
 Inoue, K. T. & Chiba, M. 2004, astro-ph/0411168
 Keeton, C. R., Gaudi, B.S., & Petters, A. O., 2003, ApJ, 598, 138
 Keeton, C. R., 2003, ApJ, 584, 664
 Klypin, A., Kravtsov, A. V., Valenzuela, O., & Prada, F. 1999, ApJ, 522, 82
 Mao, S. & Schneider, P. 1998, MNRAS, 295, 587
 Metcalf, R. B., & Madau, P. 2001, ApJ, 563, 9
 Metcalf, R. B. & Zhao, H. 2001, ApJ, 563, 9
 Metcalf, R. B. & Zhao, H. 2002, ApJ, 567, L5
 Metcalf, R. B., 2004, astro-ph/0412538
 Moore, B., Ghigna, S., Governato, F., Lake, G., Quinn, T., & Stadel, J. 1999, ApJ, 524, L19
 Navarro, J. S., Frenk, C. S. & White, S. D. M. 1996, ApJ, 462, 563
 Wiklind, T. & Alloin D., 2002, Lect. Notes. Phys., 608, 124
 Wiklind, T., 2003, ApJ, 588, 736
 Yonehara, A., Umemura, M. & Susa, H. 2003, PASJ, 55, 1059

⁴ ALMA homepage: <http://www.eso.org/projects/alma/science/bin/sensitivity.html>

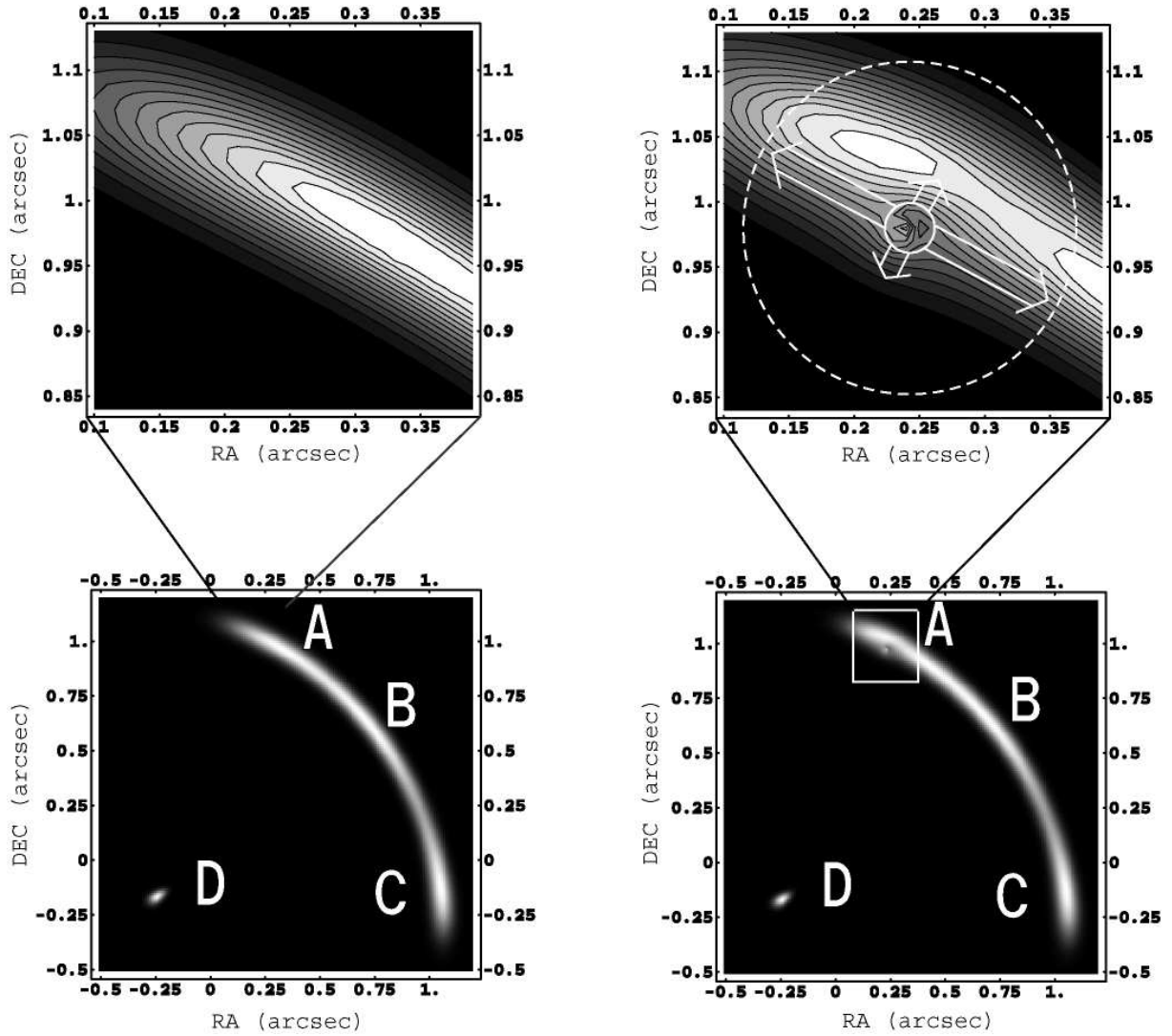


FIG. 1.— Simulated images of B1422+231 at submillimeter wavelengths without any perturbations (left) with an SIS perturber (right) for a gaussian circular source with a standard deviation $L = 2.5 \times 10^2$ pc. A tidally truncated SIS with a mass $2 \times 10^8 M_{\odot}$ is put at the center of a thick circle (upper right) near the A image. The dashed circle represents a circle with the tidal radius centered at an SIS perturber. Angular resolution is assumed to be 0.01arcsec. Astrometric shifts in the tangential direction and those in the radial direction in the coordinates aligned to the shear are represented by arrows.

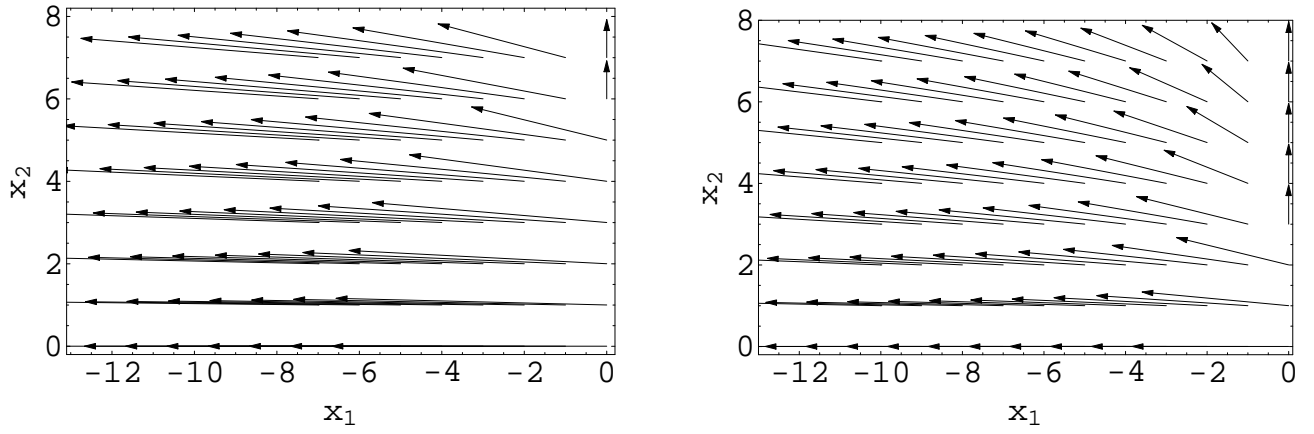


FIG. 2.— Astrometric shifts $\Delta \mathbf{x}$ for an SIS perturber in a macrolens halo for $\beta = 0$ (left) and that for an SIS perturber in the foreground of a macrolens for $\beta = 0.5$ (right) with respect to images for an unperturbed macrolens in the image plane (x_1, x_2) aligned to the shear. The both horizontal and vertical axes are normalized by an Einstein radius θ_{E_p} of an SIS perturber. We adopt a convergence $\kappa = 0.38$ and a shear $\gamma = 0.47$ for a macrolens.

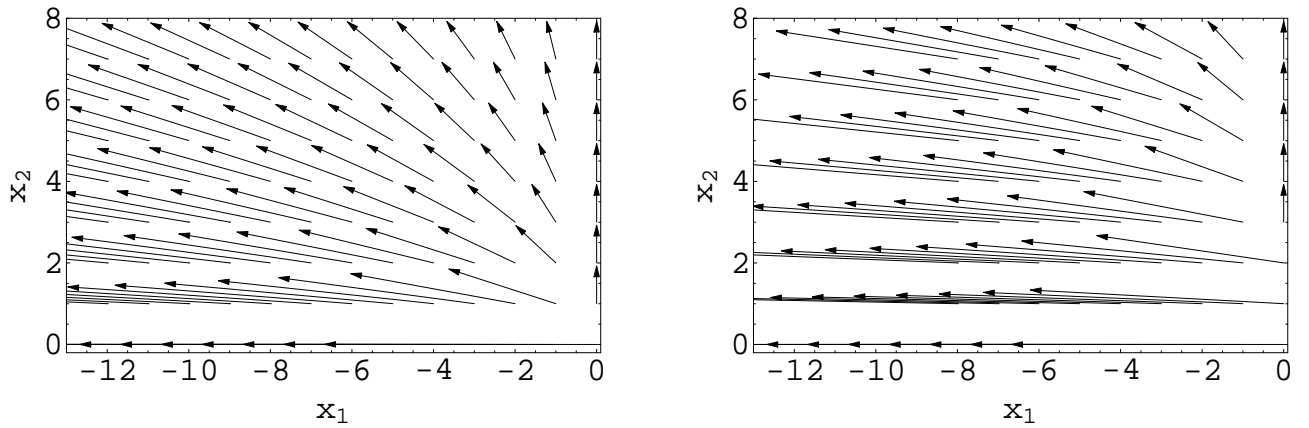


FIG. 3.— Astrometric shifts $\Delta \mathbf{x}$ for an SIS perturber in the background of a macrolens halo for $\beta = 0.9$ (left) and $\beta = 0.5$ (right) with respect to images for an unperturbed macrolens model. The other parameters are the same as those in Figure 2.